ARTICLE

A diamagnetic iron complex and its twisted sister – Structural evidence on partial spin state change in a crystalline iron complex†

Received 00th January 20xx,
Accepted 00th January 20xx

DOI: 10.1039/x0xx00000x

Esko Salojärvi,[a] Anssi Peuronen,[a] Jani Moilanen,[b] Hannu Huhtinen,[c] Johan Lindén,[d] Akseli Mansikkamäki,[e] Mika Lastusaari[a] and Ari Lehtonen[a*]

We report here the syntheses of a diamagnetic Fe complex [Fe(HL)$_2$] (**1**), prepared by reacting a redox non-innocent ligand precursor N,N'-bis(3,5-di-*tert*-butyl-2-hydroxy-phenyl)-1,2-phenylenediamine (H_4L) with $FeCl_3$, and its phenoxazine derivative [Fe(L')$_2$] (**2**), wich was obtained via intra-ligand cyclisation of the parent complex. Magnetic measurements, accompanied by spectroscopic, structural and computational analyses show that **1** can be viewed as a rather unusual Fe(III) complex with a diamagnetic ground state in the studied temperature range due to a strong antiferromagnetic coupling between the low-spin Fe(III) ion and a radical ligand. For a paramagnetic high-spin Fe(II) complex **2** it was found that, when crystalline, it undergoes a thermally induced process where 25 % of the molecules in the material change to a diamagnetic low-spin ground state below 100 K. Single crystal X-ray studies conducted at 95 K afforded detailed structural evidence for this partial change of spin state of **2** showing the existence of crystallographically distinct molecules in 3:1 ratio which exist in high- and low-spin states, respectively. Also, the magnetic behaviour of **2** was found to be related with the crystallinity of the material as demonstrated by near-IR radiation to unpaired electrons conversion ability of amorphous sample of **2**.

Introduction

The chemistry of base metal complexes with redox non-innocent ligands (NILs) – *i.e.* ligands that can exist in multiple different oxidation states and as a result cause an ambiguity in determining the oxidation state of the central metal – has been a matter of significant interest among chemists for a while. Complexes with redox-rich metal ions are of particular interest as such complexes can exhibit intricate electron transfer processes at mild potentials. This behaviour can manifest as intense absorption in near-IR region and result in energetically close-lying redox states, which can be thus utilised in molecular sensing[1] or molecular memory[2] applications. For example, earlier studies on d-block metal complexes[3–8] of an archetypical redox non-innocent ligand *N*,*N*'-bis(3,5-di-*tert*-butyl-2-hydroxy-phenyl)-1,2-phenylene-diamine H_4L (from hereon L corresponds to the ligand in any oxidation state) show that this proligand can form 1:1 or 2:1 complexes with a variety of transition metals wherein the oxidation state of the ligand varies from 0 to −4 (Scheme 1). These complexes are actively studied as metalloenzyme-mimetic catalysts, molecular magnets as well as in photovoltaic applications.[9–11] Besides the redox processes and the formation of radical species, H_4L can undergo other structural reorganisations upon coordination. Notably, Lesh *et al.* have demonstrated that an intra-ligand cyclisation occurs when H_4L is reacted with a Co(II) precursor in basic oxidizing conditions to yield [Co(L')$_2$], a low-spin Co(III) complex of phenolate/phenoxazinyl (PhO^-–N^-–$Phz^\bullet$) radical ligand species.[7] This behaviour of Co with H_4L was distinguishable from that of Mn or Fe, which, under similar conditions, did not result in ligand rearrangement but gave uncyclized [Mn(HL)$_2$] and [Fe(L)Cl] complexes, respectively. In this report, we present new evidence regarding the reactivity of H_4L by demonstrating its tendency to undergo cyclisation in a controlled stepwise manner starting from a pre- prepared uncyclized [Fe(HL)$_2$] complex **1** which, following a ligand rearrangement, gives the respective phenoxazinyl iminophenolate [Fe(L')$_2$] complex **2**. As will be shown, **2** exhibits properties in the solid state that can be associated either to the occurrence of valence tautomerism (VT) or spin crossover (SCO) processes. In VT, the combination of redox-active ligands and metal ions with two or more available oxidation states leads to two nearly degenerated electronic states with localized electronic structures.[12] Charge distributions in these tautomers are prone to the external stimuli and intramolecular electron transfer between the redox active units may be caused e.g. by

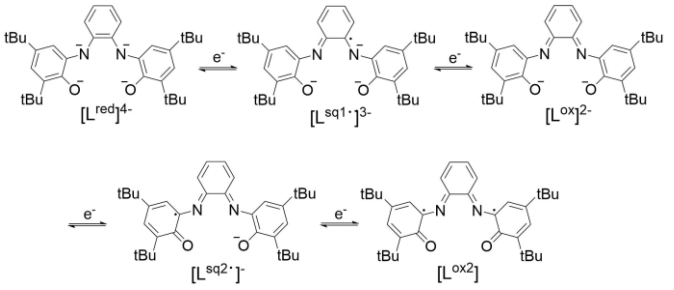

Scheme 1. The different oxidation states of the deprotonated ligand L (adopted from the reference 6).

[a]*Inorganic Materials Chemistry research group, Department of Chemistry, University of Turku, FI-20014 Turku, Finland*
[b]*Department of Chemistry, P.O. Box 35, University of Jyväskylä, FI-40014 Jyväskylä, Finland*
[c]*Wihuri Physical Laboratory, Department of Physics and Astronomy, University of Turku, FI-20014 Turku, Finland*
[d]*Faculty of Science and Engineering/Physics, Åbo Akademi University FI-20500, Turku/Åbo, Finland*
[e]*NMR Research Unit, University of Oulu, P. O. Box 3000, 90014 Oulu, Finland*
†Electronic Supplementary Information (ESI) available: Details of experimental methods and synthesis, crystallographic data tables and additional figures. CCDC

light irradiation, or change in pressure or temperature. SCO compounds are capable to reversible switch from a low-spin (LS) electronic state to a high-spin (HS) electronic state. Again, several external effects, such as temperature, pressure, photons and magnetic field, can induce this spin state change.[13] A VT process is known to occur for some Mn, Fe and Co complexes,[14–18] but generally in solution and not in the solid state at low temperatures. On the other hand, it is known that several Fe(II) complex with N_4[19], N_4S_2[20] and N_2O_2[21–23] donor sets can display crystal packing dependent SCO phenomena.

Experimental section

Methods and Materials

The ligand precursor was synthesized by literature procedures.[5,8] Other chemicals were used as purchased from commercial sources. The solvents used were of HPLC grade. All syntheses were done under an ambient atmosphere.

The FTIR spectra of powder samples of **1** and **2** were recorded with Bruker VERTEX 70 FTIR spectrometer equipped with a HarrickVideo MVP™ diamond ATR accessory. The ^{1}H and ^{13}C NMR spectra were recorded with 500 Mhz Bruker AVANCE-III NMR-system (^{1}H: 500 MHz, ^{13}C: 126 MHz) equipped with a broad-band smart probe. ESI-MS for complexes were measured in the positive-ion mode with a Bruker micrOTOF-Q spectrometer. The samples were injected as acetonitrile or dichloromethane solutions. Thermal changes, including melting points, decomposition temperatures and possible inclusion of crystallisation solvent, of the complexes were studied with a TA Instruments SDT Q600 simultaneous TGA-DSC apparatus between 23 and 500°C in flowing nitrogen gas, using an aluminium oxide pan as a sample holder. Flow rate of the gas was 100 mL/min and the samples (9.76 mg of **1**, 9.13 mg of **2**, respectively) were heated with the rate of 5° C/min. Mass loss and heat flow traces of **1** and **2** are presented in Figures S19 and S20. UV/vis–spectra in CH_2Cl_2 solutions were measured with Agilent Cary 60 UV/vis spectrophotometer. The powder and frozen glassy toluene solution X-band EPR spectra of **1** and **2** were recorded at 77 K and 293 K using Magnettech MiniScope MS 200 spectrometer (Magnettech, Berlin, Germany). Toluene solvent was dried by refluxing it over sodium and degassed with three freeze-pump-thaw cycles. Ca. 5.0×10^{-4} M solutions of samples were prepared, degassed prior to the measurements and kept under a vacuum in the J. Young EPR sample tubes.

Magnetic measurements: The magnetic properties were measured in a SQUID magnetometer. The temperature dependence of the zero-field-cooled (ZFC) and field-cooled (FC) magnetization was measured at 2 - 300 K with a Quantum Design SQUID magnetometer MPMS XL with the external magnetic field of B = 1.0 T. 29.11 mg, 27.21 mg and 45.42 mg samples of **1**, **2** (crystalline) and **2** (amorphous) respectively, were sealed in plastic nonmagnetic straws. The theoretical diamagnetic atomic constants were subtracted from the measured and calculated values of the molar magnetic susceptibility of the crystalline sample of **2**. The field dependence was measured at 2 K between −5.0 and 5.0 T using 50 mT steps. Virgin magnetizations as a function of B and magnetic hysteresis curves were recorded in magnetic fields up to 5 T at temperatures of 2, 30, 50, 100 and 300 K. Although the magnetic particles were randomly oriented on the surface of the substrate, the external magnetic field B was always oriented along the out-of-plane axis of the substrate.

The photoinduced magnetization measurements were performed in dark or under illumination through an optical fibre with a homemade fibreoptic sample holder attached to the SQUID magnetometer. The samples of **1** and **2** were drop casted as diethyl ether solutions on circular $SrTiO_3$ plates (diameter 5 mm). The light source was a Fabry-Perot laser diode by Thorlabs operating at λ = 785 nm (1.58 eV) with a maximum output power of 10 mW measured at the end of the optical fibre, and hence, the laser flounce on the sample surface was ca. 0.5 mW/mm^2.

Mössbauer measurements: ^{57}Fe Mössbauer spectra were recorded with Doppler velocities Ca. 3.0 mm/s and calibrated using α-Fe. Spectra were measured in transmission geometry in the temperature interval 77-315 K using an Oxford CF506 continuous-flow cryostat with liquid N_2 as coolant and a ^{57}Co:Rh source (Ritverc Co. 25mCi June 2018). The spectra were fitted using a homemade nonlinear least-squares fitting program with the following Mössbauer parameters released in the fitting: the quadrupole coupling constant eQV_{zz}, the relative component intensities, and the isomer shift δ relative to α-Fe. The hyperfine parameters due traces of Fe in the beryllium window of the detector were kept fixed during the analysis.

Single crystal X-ray diffraction analyses: The data collections were carried out using Agilent SuperNova microfocus dual source (Cu/Mo) diffractometer equipped with an Atlas detector. The data collection and reduction, including multifaceted crystal model based analytical absorption correction, were carried out using CrysAlis^{pro} program[24]. The structures were solved with ShelXS[25] using direct methods and refined on F^2 by full matrix least squares techniques using ShelXL[26] within the Olex^2 (v. 1.2.10)[27] program package. All non-hydrogen atoms were refined anisotropically. The hydrogen atoms were refined using a riding model with fixed thermal parameters 1.2-1.5 times the values of the corresponding host atoms (the O–H distances of the O2 and O4 hydroxyl groups were refined freely). Both crystal structures show ca. 100 Å^3 of void space in their unit cells. These small voids did not show any significant residual electron density and thus they are most likely a result of solvent molecules escaping the crystal lattice prior to XRD analyses or innate cavities present in the crystal structures.

Computational details: The geometries of **1** and **2** (both 120 K and 95 K crystal phase) were extracted from the respective crystal structures. The positions of the hydrogen atoms were optimized using density functional theory (DFT) while the positions of heavier atoms were kept frozen to their crystal-structure coordinates. The energies of the high-spin (S = 2) and low-spin (S = 0) states were calculated for **1** and for all complexes in the asymmetric unit of the high- and low-temperature crystal structures of **2**. The calculated energies are listed in Table S5.

All calculations were carried out using the *Orca* quantum chemistry code version 4.2.1.[28,29] The pure generalized gradient approximation PBE to the exchange-correlation (XC) functional[30,31] was used in the optimization of the hydrogen positions whereas the CAM-B3LYP range-separated hybrid XC functional was used in the energy evaluations.[32–34] Scalar relativistic effects were introduced using the standard second-order Douglas–Kroll–Heß (DKH) transformation.[35,36] Re-contracted versions of def2 basis sets specifically designed for DKH calculation (DKH-def2) were used in the calculations. A polarized double-ζ-quality basis (DKH-def2-SVP) was used in the geometry optimizations whereas a polarized triple-ζ-quality basis (DKH-def2-TZVP) was used in the energy evaluations.[37,38] The resolution-of-identity (RI) approximation was used in the geometry optimizations utilizing the SARC/J auxiliary basis set.[37]

Synthetic procedures

Preparation of 1: Anhydrous $FeCl_3$ (150 mg, 0.925 mmol), H_4L (870 mg, 1.68 mmol) and 300 µL of NEt_3 were left to stand in a sealed vessel in MeOH (40 mL) for 2 days. Precipitated dark solid was dissolved in CH_2Cl_2, filtered and recrystallized from a CH_2Cl_2/MeOH solution. Yield 622 mg (68 %, based on the ligand). Anal. Calcd for $C_{68}H_{90}FeN_4O_4$: C, 75.39; H, 8.37; N, 5.17. Found: C, 75.57; H, 8.55; N, 4.88. IR: 2952 (s), 1520 (w), 1478 (m), 1433 (m), 1361 (s), 1303 (s), 1246 (vs), 1200 (m), 1132 (vs), 1025 (m), 992 (m), 914 (m), 878 (m), 857 (m), 824 (m), 775 (m), 737 (s), 679 (m), 641 (m), 594 (s), 554 (m), 501 (m) cm^{-1}. ^1H NMR ($CDCl_3$): δ 6.93 (d, J_{HH} = 1.76 Hz, 2H, Ph-H), 6.44 (d, J_{HH} = 8.99 Hz, 2H, Ph-H), 6.33 (s, 2H, Ph-H), 6.13 (s, Ph-OH), 5.35 (d, J_{HH} = 1.86 Hz, 2H, Ph-H), 4.98 (d, J_{HH} = 9.09 Hz, 2H, Ph-H), 4.94 (s, 2H, Ph-H) 4.77 (t, J_{HH} = 7.25 Hz, 2H, Ph-H), 4.44 (q, J_{HH} = 2.04 and 6.82 Hz, 2H, Ph-H), 1.32, 1.17, 1.06 (3s, 72H, $C(CH_3)_3$), ppm. ^{13}C NMR ($CDCl_3$): δ 175.25, 165.45, 155.82, 143.00, 139.59, 136.77, 136.22, 135.65, 135.50, 134.22, 132.71, 130.36, 126.51, 123.00, 119.63, 116.31, 116.21, 115.21 (Ph-C) 35.99, 35.01, 34.80, 33.27 ($C^*(CH_3)_3$), 32.60 31.77, 29.38, 28.87 ($C(C^*H_3)_3$) ppm. ESI(+)-MS: (MeCN): *m/z* 1078.6001 $[M\text{-}4H(\text{two ligand reformation})]^+$ calcd. *m/z* 1078.5993), *m/z* 1082.6250 $[M]^+$ calcd. *m/z* 1082.6306. (CH_2Cl_2): *m/z* 1082.6559 $[M]^+$ calcd. *m/z* 1082.6306. m.p. 280 °C (decomp.).

Preparation of 2: 570 mg (0.53 mmol) of **1** was refluxed overnight (20 h) in a basic acetonitrile solution (50 mL of MeCN and 2 mL of NEt_3). The mixture was evaporated to dryness with a rotary evaporator, then dissolved in diethyl ether and filtered through a silica plug. X-ray quality crystals were obtained by recrystallization from MeOH/Et_2O mixture. Isolated yield of dark crystals was 162 mg. (28 %). Anal. calcd. for $C_{68}H_{86}FeN_4O_4$: C, 75.67; H, 8.03; N, 5.19. Found: C, 75.16; H, 8.16; N, 5.09. IR: 2952 (s), 2903 (m), 2866 (m), 1757 (w), 1605 (m), 1569 (w), 1530 (s), 1478 (s), 1461 (m), 1438 (m), 1410 (m), 1392 (m), 1361 (s), 1336 (s), 1293 (m), 1279 (m), 1252 (vs), 1220 (s), 1198 (s), 1155 (s), 1113 (s), 1083 (vs), 1048 (s), 1022 (s), 989 (s), 954 (m), 930 (m), 909 (s), 870 (m), 849 (w), 836 (w), 809 (w), 789 (w), 771 (s), 758 (s), 730 (s), 678 (s), 661 (m), 624 (s), 610 (s), 594 (s), 566 (s), 534 (s), 503 (s) cm^{-1}. ESI(+)-MS: (MeCN): *m/z* 1078.6001 $[M]^+$ calcd. *m/z* 1078.5993), *m/z* 1079.6017 $[M+H]^+$ calcd. *m/z* 1079.6071), (CH_2Cl_2): *m/z* 1078.6025 $[M]^+$ calcd. *m/z* 1078.5993), *m/z* 1080.6129 $[M+2H(\text{one ligand reformation})]^+$ calcd. *m/z* 1080.6150), ESI(-)-MS: (MeCN): *m/z* 1078.5827 $[M]^-$ calcd. *m/z* 1078.6004). m.p. 290 °C (decomp.).

Preparation of amorphous sample of 2: A recrystallized sample of **2** was dissolved in hexane, filtered and the solution was rapidly evaporated by rotary evaporator. The low crystallinity of the obtained solid sample was confirmed by a powder XRD measurement.

Results and discussions

Synthesis and characterisation of 1

$FeCl_3$ reacted with two equivalents of ligand precursor H_4L in a MeOH solution (Scheme 2) under ambient conditions to form a dark brown solution. Black crystals that precipitated were further purified by recrystallization and isolated in a 68 % yield. The ^1H NMR spectrum of **1** in $CDCl_3$ at room temperature displayed chemical shifts for one distinct ligand, which confirms that the ligands are symmetrically equivalent and the complex itself is diamagnetic in solution. Interestingly, electrospray mass spectrometric (ESI-MS) analysis of **1** in ESI-MS(+) mode gave an expected peak pattern in CH_2Cl_2 whereas a non-characteristic isotope distribution was observed in MeCN in (see figures S2-S6 in ESI). The peak distribution suggests that the pattern arising from $[\mathbf{1}]^+$ with *m/z* = 1082.6250 is partially overlapped by another Fe-species with an *m/z* value of 1078.6001 corresponding to **1** with four less H atoms. This suggests that the ligands have the tendency to react by similar intramolecular cyclisation, as reported by Lesh et al. for the Co complex.[7] This reactivity will be discussed below. The magnetic properties of **1** were studied by SQUID magnetometry. As expected on the grounds of the well-resolved NMR spectra, **1** shows a diamagnetic signal (Fig. S11). Similarly, the powder and frozen glassy toluene X-band EPR spectra of **1** were measured in the magnetic field range of 50-450 mT at 77 K and 293 K but no signal was detected, which is fully in line with the magnetic SQUID data and underpins the diamagnetic nature of **1** in the entire scanned temperature range.

Single-crystal X-ray diffraction analysis showed that complex **1** crystallises in the $P\bar{1}$ space group with one molecule in the asymmetric unit (see ESI for experimental details). The complex is mononuclear with six donor atoms from two triply deprotonated tridentate ligands occupying the coordination sphere around the metal centre, while one phenol OH from each of the ligands remains protonated and forms an intramolecular interligand hydrogen bond. The phenolate O

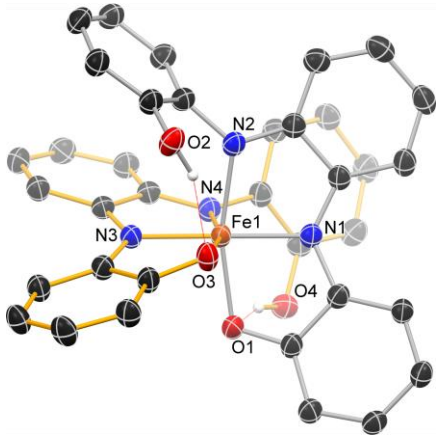

Figure 1. The molecular structure of 1 determined by single crystal X-ray. Displacement ellipsoids are presented at 50% probability level. *tert*-Butyl groups and C–H H atoms are omitted for clarity. List of selected bond parameters: Fe1–O1 = 1.9470(12), Fe1–O3 = 1.9579(11), Fe1–N1 = 1.8760(13), Fe1–N2 = 1.9692(14), Fe1–N3 = 1.8744(13), Fe1–N4 = 1.9616(13).

atoms are coordinated in a *cis* arrangement resulting in an approximately C_2-symmetric complex, thus explaining the observed equivalency of the ligand proton shifts in the ^{1}H NMR spectrum in solution. The rather short Fe–O and Fe–N distances suggest that the Fe ion is at a low-spin (LS) state. At this point, it is worthwhile to establish that there are several possible combinations of formal oxidation states the Fe centre and the two ligands in **1** can express taken account that **1** was found to be diamagnetic in solution. Intuitively, a LS Fe(II) centre with two $[HL^{ox}]^{-1}$ ligands seems as the most obvious assignment of the charges within complex **1**. Assuming a LS Fe(II) ion, another possible configuration of ligand charge and spin involve $[HL^{sq1\bullet}]^{2-}$ antiferromagnetically coupled with a neutral $[HL^{sq2\bullet}]$. Alternatively, the complex can be described as a combination of LS Fe(III) ion and $[HL^{ox}]^{1-}$ and $[HL^{sq1\bullet}]^{2-}$ ligands wherein the radical ligand is antiferromagnetically coupled to the S = ½ low-spin Fe(III). Furthermore, a diamagnetic complex can also be obtained by the combination of LS Fe(III), $[HL^{red}]^{3-}$ and $[HL^{sq2\bullet}]$.

It has been well established that the different *o*-amidophenoxide oxidation states, from 0 to –2, can be distinguished by analysing the respective C–O, C–N and C–C bond distances by the aid of high-quality X-ray crystal structure.[39] A convenient measure of the oxidation state, namely "metrical oxidation state" (MOS), has been proposed by Brown,[40] which is based on bond length correlations in a statistical analysis of a large set of mono- and unconjugated bis(*o*-amidophenoxide) ligands. For the two nearly identical ligands in **1**, the MOS calculation yielded values –1.419(8) and –1.534(7), which translate roughly into a non-integer oxidation state of –1.5 for each of the ligands. A reasonable interpretation MOS parameters would be to describe the complex with an averaging of two localised forms, $[HL^{ox}]^{1-}$ and $[HL^{sq1\bullet}]^{2-}$, resulting in Fe(III) formal oxidation state. However, the reliability of the MOS parameter in describing the oxidation state of a conjugated ligand, such as $[HL]^n$ may have issues since such ligands were not included in the MOS parameter set. Therefore, we decided to further compare the bond parameters

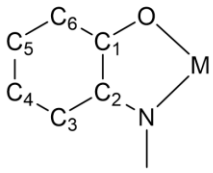

	Fe	Ni
C_1–O	1.325(2), 1.334(3)	1.298(2), 1.308(3)
C_2–N	1.388(2), 1.392(3)	1.375(2), 1.363(3)
C_1–C_2	1.423(3), 1.420(2)	1.462(3), 1.430(3)
C_2–C_3	1.403(2), 1.404(3)	1.418(2), 1.428(3)
C_3–C_4	1.377(2), 1.379(3)	1.377(3), 1.359(4)
C_4–C_5	1.416(3), 1.411(3)	1.441(3), 1.407(3)
C_5–C_6	1.386(2), 1.389(3)	1.372(3), 1.385(4)
C_6–C_1	1.423(2), 1.418(3)	1.445(3), 1.430(4)

Figure 2. Comparison of *o*-amidophenoxide bonding parameters between **1** (Fe) and $Ni(HL)_2$ (from ref. 42). Bond lengths are reported in Å for both discrete *o*-amidophenoxide moieties of each complex.

of **1** to other known $M(HL)_2$ type complexes in which the ligands have been unambiguously assigned to exist in the $[HL^{ox}]^{1-}$ form. According to the Cambridge Structural Database (CSD), five $M(HL)_2$ type complexes have been structurally characterised earlier. In three of these the metal ions (V, Mo and W) show oxidation states higher than +2,[6,41,42] whereas in one (Mn) the oxidation state has not been assigned.[43] However, a paramagnetic nickel(II) complex, investigated earlier by us and which is also isostructural with **1**,[42] is a suitable comparison. The relevant average heteroatom–carbon and carbon–carbon distances in $Ni(HL^{ox})_2$ and **1** are presented in Figure 2. The changes in the oxidation states of the ligands are seen by observing the C–O, C–N, C_1–C_2 and C_4–C_5 interatomic distances. Increase of negative charge on the ligand elongates the carbon-heteroatom distances while the two carbon-carbon distances are shortened. This effect is evident when observing the relevant interatomic distances of **1** in comparison to $Ni(HL^{ox})_2$, which suggests that the ligands in **1** deviate from the $[HL^{ox}]^{1-}$ form and toward a structure where more negative charge is localised in the ligands. The evaluation of bond parameters therefore provides further evidence on the interpretation according to which the structural features of the complex can be explained by using a "$[HL^{ox}]^{1-}$–Fe(III)–$[HL^{sq1\bullet}]^{2-}$" formulation. To have more evidence on the oxidation state of the iron centre, Mössbauer measurements were performed on the solid-state sample of **1** (Table 1). The spectrum exhibits one Fe-containing component. The observed signal is compatible with LS Fe(III) ion, as the true isomer shift is 0.1139(1) mm/s obtained from Debye fitting the isomer-shift data. The fitted Debye temperature is 800(20) K. These are rather high values and in contrast to what is obtained when fitting the absorption area: 158(2) K. No signs of temperature-dependent spin crossover were observed for **1** in the solid state. Altogether, both the XRD structural parameters and the Mössbauer spectrum suggest that complex **1** consists of a Fe(III) ion and an organic radical – via the $[HL^{ox}]^{1-}$/$[HL^{sq1\bullet}]^{2-}$ resonance structure of the two ligands – with the unpaired electron antiferromagnetically coupled with the LS Fe(III) centre in order to have a diamagnetic molecular complex. This is fully in-line with the observations from the NMR spectra and XRD studies which indicate two identical ligands. Actually, this behaviour is not unique within *o*-amidophenoxide type complexes as demonstrated by Mukherjee and co-workers using a diamagnetic Fe(III) complex with an apparent resemblance to **1**.[18]

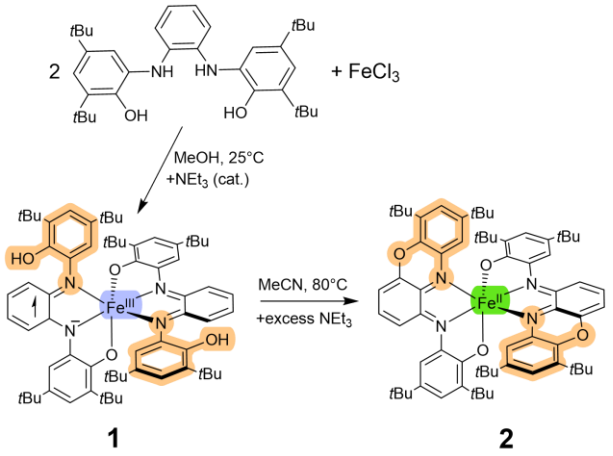

Scheme 2. Formation of **1** and **2** and the proposed oxidation states of the Fe centres and ligands, respectively. **1** is drawn as a presentation of one of the two equivalent cases where the unpaired electron is localised at one of the two ligands. Structure of **2** reflects the structural features observed above 95 K.

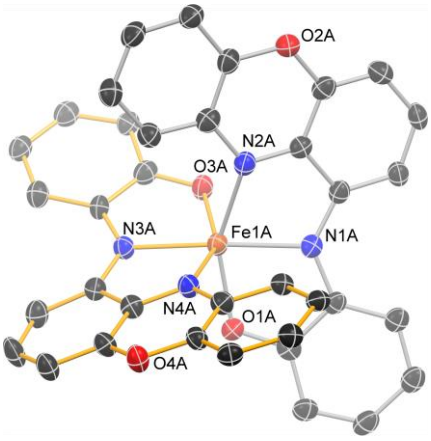

Figure 3. The molecular structure of **2** determined by single crystal X-ray at 120 K. Only one of the two discrete molecules in the asymmetric unit is drawn. Displacement ellipsoids are presented at 50% probability level. *tert*-Butyl groups and C–H H atoms are omitted for clarity. Fe1A–O1A = 1.998(3), Fe1A–O3A = 2.013(3), Fe1A–N1A = 2.079(4), Fe1A–N2A = 2.133(4), Fe1A–N3A = 2.075(4), Fe1A–N4A = 2.145(4).

Synthesis and molecular structure of 2.

As declared above, complex **1** may react in solution via an intramolecular reaction, as realised from the MS-measurements. Indeed, when a sample of **1** is refluxed overnight in a basic MeCN solution under ambient atmosphere, the ligands undergo a structural reorganization involving intramolecular cyclisation (see Scheme 2) to yield complex **2**.‡ The reaction mixture was evaporated, and the complex was recrystallized from MeOH/Et_2O to obtain high-quality crystals for XRD analyses. The compound was found NMR silent in $CDCl_3$ solution and was thus assumed paramagnetic. The solid-state structure of **2** was determined by X-ray diffraction at 120 K, which showed that the intra-ligand cyclisation had resulted in the formation of a complex with two types of Fe–N bonds; two occur to the phenoxazinyl moieties, which are in the range of 2.12-2.15 Å, and two to the amino nitrogens with Fe–N distances within 2.05-2.08 Å for the two distinct molecules in the asymmetric unit. The observed Fe–N and Fe–O distances in **2** are *ca.* 0.2 and 0.1 Å longer, respectively, compared to the analogous distances in the related low-spin Co(III) complex, whereas the overall structure is otherwise very similar.[7] The long Fe–N and Fe–O distances suggest that the complex consists of a high-spin Fe ion, whereas its formal oxidation state can be estimated from the ligand interatomic distances by calculating the MOS parameters of the *o*-amidophenoxide moieties. For the two discrete complexes in the crystal structure of **2** the MOS values were calculated as –1.191(7) and –1.261(6), and –1.017(9) and –1.307(16), respectively. While the MOS parameter is not expected to accurately depict the oxidation state of a phenoxazinyl amidophenoxide type ligand, which formally consists of two redox-active parts, they perform rather well in the case of an analogous Co(III) complex for which MOS calculations yield very close to expected values of –1.506(6) and –1.323(4).[7] Hence, although not conclusive, based on the structural data at 120 K, it is reasonable to suggest that **2** consists of a high-spin Fe(II) ion and two monoanionic ligands (Scheme 2). This interpretation is further warranted by DFT calculations (see below) and the metal-donor bonding distances which are comparable to high-spin Fe(II) complexes with monoanionic ONN ligands.[44] When the structure determination of **2** was repeated at 95 K – which was done due to the observed phenomenon in the $\chi T/T$ curve at 100 K (see below) – a change

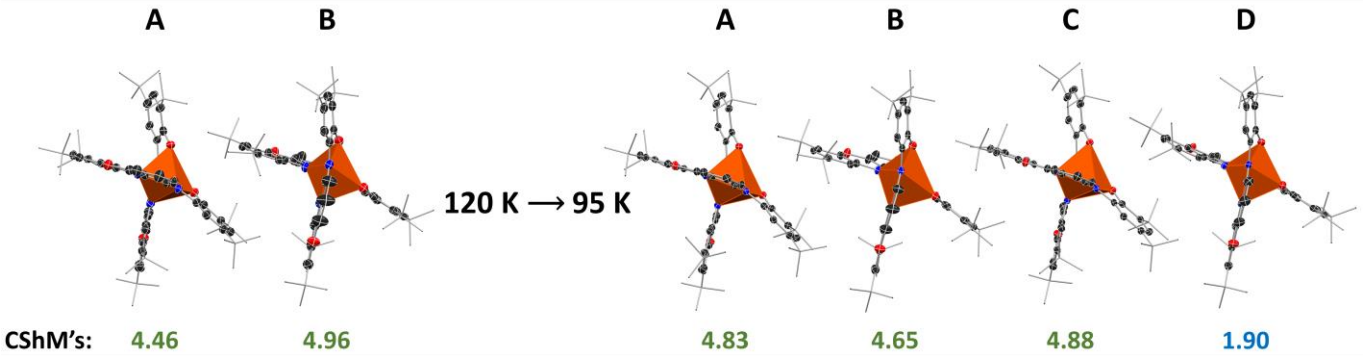

Figure 4. Illustration of the two asymmetric units found in the crystal structures of **2** measured at 120 K (left) and 95 K (right). Below each discrete molecule a Constant Shape Measure (CShM) value, calculated by comparing each coordination environment to an ideal octahedron structure, is reported, showing the significant difference of the coordination geometry of molecule **D** at 95 K to all other molecules.

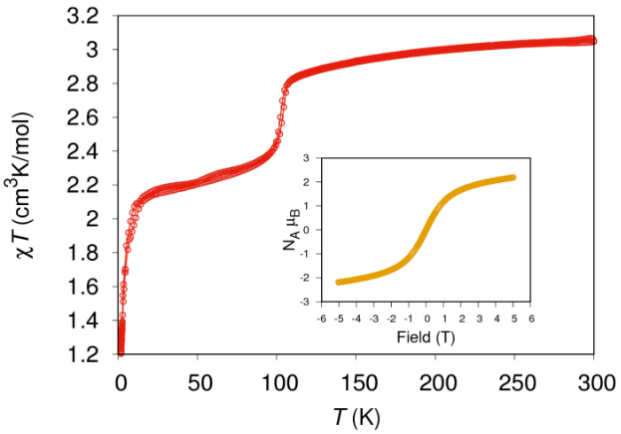

Figure 5. The χT values as the function of temperature in the crystalline sample of **2**. The inset represents the field dependence curve at 2 K.

in the crystal structure was observed underlined by a sudden appearance of significant disorder along almost the entire molecular backbones of both discrete complexes present in the asymmetric unit. Further analysis revealed that the structure at 95 K is best solved and refined using a unit cell with double the volume compared to the 120 K structure and by establishing the space group setting $P2_1/c$ rather than $P2_1/n$. This gives an asymmetric unit with four distinct well-resolved molecules, three of which (with suffix **A**-**C**) display nearly identical Fe–L bond distances compared to the two discrete molecules in structure of **2** determined at 120 K (Figure 4 as well as Figure S1 and Table S4 in ESI). In contrast, in the fourth molecule (**D**), the Fe–L bond lengths are significantly shorter and correspond to 0.05, 0.165 and 0.156 Å decrease in Fe–$O_{phenolato}$, Fe–N_{amine} and Fe–$N_{phenoxazinyl}$ bond lengths, respectively, when compared to the respective average Fe–L distances in molecules **A**-**C**. These differences are also highlighted by the calculated Continuous Shape Measures (CShMs) for each or the coordination environments, which point out close similarity between the coordination geometry of molecules **A**-**C** and their difference to molecule **D** (Figure 4, ESI Table S4). All four coordination environments are best described using an octahedron reference shape with molecules **A**-**C** distorted more towards trigonal prism than molecule **D**. The observations made based on the crystal structure data point to a thermally induced SCO or VT process in which every fourth molecule in the crystal lattice of **2** has experienced a change in either the oxidation state or spin state of the central Fe ion. The Metrical oxidation states calculated for molecules **A**-**C** fall within –1.02 and –1.17 whereas slightly more negative values of –1.325(13) and –1.197(8) are calculated for molecule **D**, latter of which do not unambiguously point out to either Fe(II) or Fe(III) ion. However, the shortening of the metal–ligand bonds in molecule **D** of **2** at

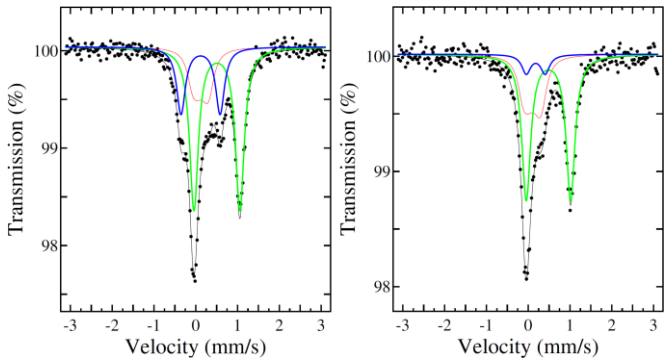

Figure 6. The Mössbauer spectra of crystalline sample of **2** measured at 77 K (left) and 140 K (right). The red signals are due to an instrumental artifact.

95 K strongly suggest that a partial spin-crossover from high-spin to low-spin Fe ion has occurred for 25% of the molecules in the material during the thermally induced single-crystal-to-single-crystal transition.

Magnetic properties and Mössbauer spectroscopy of 2

SQUID magnetometry were used to obtain more information on the magnetic properties of **2**. The χT value of a crystalline sample of **2** (Figure 5) shows a slow decrease as the sample is cooled from 300 K until an abrupt drop occurs at ca. 100 K. Above this temperature the χT value varies around 2.8-3.0 cm^3 K mol^{-1} while between ca. 10-100 K the χT value varies around 2.0-2.3 cm^3 K mol^{-1}, former of which corresponds the theoretical spin-only value of 3.00 cm^3 K mol^{-1} calculated for HS Fe(II) with diamagnetic ligands (S = 2). In other words, the $\chi T/T$ data suggest that cooling below 100 K induces a sudden decrease in the total number of unpaired electrons in the material. This event is in line with the observed single-crystal-to-single-crystal phase transition in the XRD measurements, associated with the spin-crossover from high- to low-spin Fe for 25% of the molecules.

The powder and frozen glassy toluene X-band EPR spectra for **2** were measured in the magnetic field range of 50-450 mT at 77 K and 293 K, however, no signal was detected. It is also expected that the one LS (S = 0) and three HS (S = 2) complexes observed in the asymmetric unit of **2** at 95 K do not give a signal in the X-band regime due to the singlet ground state of LS complex and a large zero-field splitting of non-Kramers HS Fe(II) ion, respectively. Zero-field splitting parameters of HS Fe(II) ions vary usually between 5 cm^1 and 20 cm^{-1} and, thus, their allowed EPR transitions appear in a high frequency range that is out of the capability of an X-band EPR spectrometer.[45–47] In Mössbauer spectroscopy, the crystalline sample of complex **2** exhibits one paramagnetic component above 170 K. However, at lower temperatures of 77 K, 110 K and 140 K, one additional and minor component is also detected. The minor component, representing roughly 25% of the absorption area has an isomer shift of 0.230(2) mm/s at 77 K and would thus be best described as low-spin Fe(III).[18,48–50] Upon increasing the temperature the minor component loses intensity and merges ultimately with the main component, since at 170 K the minor component is no longer detectable. At 140 K, the low-temperature component is already disappearing and the remaining doublet sits essentially

in the slopes of the main component. In this situation, the values of the quadrupole coupling constant and the isomer shift easily slide towards slightly drifting off values. Also during a transition the line width of last the remaining low-temperature phase may increase slightly (not modelled) here, which further may distort the parameter values. The isomer-shift data for the main component can be fitted using the Debye model resulting in a Debye temperature of 570(40) K and a true isomer shift of Δ_0 = 0.778(8) mm/s. The latter is too large for HS Fe(III) centre and points to a HS Fe(II) centre. These observations are consistent with the low-temperature (95 K) XRD data of **2**, according to which every fourth molecule has distinctively different bond parameters to the other three, as well as with the magnetic susceptibility data of **2** showing that a 25% diamagnetic component is mixed with 75% of HS Fe(II) complex. Furthermore, the isomer shift value for the low-spin component representing 25% of the material – also viewed as the molecule **D** in the crystal structure of **2** at 95 K – points to a case where LS Fe(III) ions are coupled to a radical ligand to yield a diamagnetic complex. The quadrupole coupling constants of the minor and the major components do not differ much, but there is an overall decrease in the quadrupole coupling constant upon increasing the temperature, probably connected with the dynamics of the local environment of the Fe centre. The total absorption area decreases very fast. In fact, a Debye fitting of the absorption area yields a very low Debye temperature of only 131(2) K.

Table 1. Zero-field Mössbauer parameters for **1** and **2**.

		1			
T (K)	δ, mm s^{-1}	eQV_{zz}, mm s^{-1}			
77.6	0.10461(5)	3.153(3)			
82	0.1060(1)	3.16(1)			
110	0.09992(5)	3.130(3)			
140	0.09231(6)	3.10(8)			
		2			
T (K)	**comp. 1**[a] δ, mm s^{-1}	**comp. 1**[a] eQV_{zz}, mm s^{-1}	**comp.2**[a] δ, mm s^{-1}	**comp.2**[a] eQV_{zz}, mm s^{-1}	Rel. intensity %
77.6	0.6226(6)	2.2(1)	0.230(2)	1.9(2)	71:29
110	0.616(5)	2.18(9)	0.227(2)	1.8(3)	75:25
140	0.601(4)	2.1(1)	0.18(9)	0.9(5)	88:12
170	0.586(3)	2.1(2)			100
200	0.571(1)	2.06(5)			100
230	0.565(5)	2.1(2)			100
260	0.55(3)	2.04(9)			100
290	0.521(7)	2.0(2)			100
315	0.519(9)	2.0(2)			100

[a]comp.1 and comp.2 refer to the two distinct components in the spectra of **2**.

Computational studies on 1 and 2

The spin-state energetics of **1** and **2** were studied further by density functional calculations at the CAM-B3LYP/DKH-def2-TZVP level. The energy difference between the HS (S = 2) and LS (S = 0) states was calculated for the crystal structure of **1** and for all complexes in the asymmetric units of both the 120 K and 95 K temperature crystal structures of **2**. As expected, the ground state of **1** is a diamagnetic LS state with the HS state lying 6805 cm^{-1} above the ground LS state. The gap between the LS and HS states is large enough that the HS state is completely depopulated at room temperature consistent with a purely diamagnetic complex.

The two complexes in the asymmetric unit of the 120 K crystal structure of **2** have a HS ground state with the LS states lying 9753 cm^{-1} and 8265 cm^{-1} above the ground state. The Löwdin spin populations of the iron ions are 4.07 and 3.98 indicating that the four unpaired electrons are localized at the Fe ion. The calculations are consistent with both complexes having HS Fe(II) ions, in agreement with the structural analyses and magnetic susceptibility as Mössbauer measurements. The three similar complexes (**A**-**C**) in the asymmetric unit of low-temperature (95 K) crystal phase of **2** have a HS ground state with the energy gaps of 10519 cm^{-1}, 7623 cm^{-1} and 8026 cm^{-1} between the HS and LS states. One of the complexes (**D**), however, has a diamagnetic LS ground state with the HS state lying only 70 cm^{-1} above the LS state. This is consistent with the interpretation of the magnetic data as 75% paramagnetic HS complexes and 25% diamagnetic LS complexes in the 95 K temperature regime. Thus, as the temperature is lowered, the transition in the crystal phase is accompanied by a transition of the magnetic state of one out of four complexes. The Löwdin spin populations of the three HS complexes **A**-**C** are 3.99, 4.04 and 4.05 consistent with HS Fe(II) ions.

Near Infra-red radiation studies of 1 and 2

Complexes **1** and **2** exhibit strong NIR absorptions in CH_2Cl_2 solution (Fig. S17), probably due to the non-innocent ligand structures and the resulting LMCT and MLCT transitions. As they appear to carry odd, potentially movable electrons, these complexes might find applications in photovoltaic devices. To find out more on the interaction of the studied complexes with NIR photons, they were studied by measuring the magnetic properties with irradiation in the NIR region using a λ = 785 nm laser diode. The samples were prepared by drop casting from Et_2O solutions on $SrTiO_3$ plates, resulting in the loss of crystallinity of the samples (see powder X-ray diffraction pattern of amorphous **2** in Figure S33). The magnetization of **1** did not change upon radiation. However, **2** exhibited increasing magnetization under 785 nm radiation, which was more profound at higher temperatures (See Fig. S24 - S29). This phenomenon can be rationalized by the excitation of molecules from lower to higher spin states, thus increasing the number of the odd electrons when irradiated with near infrared radiation. This occurs partially due to the different magnetic behaviour of crystalline versus an amorphous sample of **2**. In contrast to the crystalline material the variable temperature magnetic susceptibility data of the amorphous powder shows a rather linear and steady increase of the χT value from ca. 1.45 to 1.8 cm^3 K mol^{-1} upon raising the temperature from 2 K to room temperature. The drastic change in the magnetic properties of

2 in relation of the loss of crystallinity of the material is further demonstrated in the Mössbauer spectrum, which at 77 K, show three distinguishable components with 43.98%, 31.36% and 24.66% relative intensities (Figure S34 in ESI). Whereas these were not further analysed, the SQUID and Mössbauer measurement show that when the molecules of complex **2** are not confined into an organised crystal lattice, a mixture of multiple different spin states emerge, which result in an average spin moment of roughly $S = 1$ observed for the solid amorphous material. This can be considered as a rather complex case of valence tautomerism in action.

Conclusions

In this report, we have shown that a reaction between *N*,*N*'-bis(3,5-di-*tert*-butyl-2-hydroxy-phenyl)-1,2-phenylenediamine (H_4L) ligand precursor and $FeCl_3$ gives a diamagnetic complex $[Fe^{III}(HL)_2]$ **1**. The isolated complex undergoes an intra-ligand cyclisation in basic MeCN solution to yield a phenoxazinyl iminophenolate complex $[Fe^{II}(L')_2]$ **2**. In-depth analysis of the structural and magnetic properties of both these complexes let us to conclude that **1** can be viewed as a rather unusual Fe(III) complex with a diamagnetic ground state in the studied temperature range owing to a strong coupling of unpaired electron of a low-spin Fe(III) ion and an organic radical distributed over the two ligands. Crystalline complex **2** exists solely as a high-spin Fe(II) at temperatures above ca. 100 K (140 K according to Mössbauer data). Below this temperature a single-crystal-to-single-crystal phase transition occurs which is associated with spin-crossover from paramagnetic high-spin Fe(II) state to a structure where high-spin Fe(II) and diamagnetic complexes co-exist in 3:1 ratio as confirmed by single crystal X-ray, magnetic, Mössbauer and computational analyses.

In the absence of ordered lattice constraining the molecular geometry – i.e. in an amorphous form – the material consists of a mixture of at least three different spin states evident from the Mössbauer spectra and displays a significantly lower average spin moment compared to the crystalline material. However, when the amorphous material is illuminated with a near infrared radiation under a varying magnetic field at different temperatures, a significant increase in the magnetic moment is observed. This is explained by the conversion of light to unpaired electrons by excitation of low-spin complexes to high-spin states.

To summarise, the two studied complexes, **1** and **2**, show the fascinating chemistry resulting of combining redox non-innocent ligands with redox-active metal. By investigating the structural and magnetic properties of these complexes, several interesting phenomena were observed, including a) diamagnetic behaviour from a Fe(III) complex (**1**), b) partial thermally induced spin-crossover behaviour or c) valence tautomerism depending on the crystallinity of the material (**2**) as well as d) conversion of light to unpaired electrons (**2**). Investigations on light conversion applications of **2** and related compounds are underway in our laboratories.

Author Contributions

Esko Salojärvi: Conceptualization, investigation, methodology, visualization, writing – original draft; Anssi Peuronen: Investigation, methodology, visualization, writing – review and editing; Jani Moilanen: Investigation, methodology, writing – review and editing; Hannu Huhtinen: Investigation, methodology; Johan Lindén: Investigation, methodology; Akseli Mansikkamäki: Investigation, methodology, writing – review and editing; Mika Lastusaari: Supervision, writing – review and editing; Ari Lehtonen: Supervision, writing – review and editing.

Conflicts of interest

There are no conflicts to declare.

Acknowledgements

ES wishes to thank the Magnus Ehrnrooth and Walter Ahlström foundations for financial support and Dr. Jan-Erik Lönnqvist for elemental analysis. AP, JM and AM gratefully acknowledge the financial support by Academy of Finland (projects 315829, 320015 and 332294). AM acknowledges financial support by University of Oulu (Kvantum Institute). Computational resources were provided by CSC-IT Center for Science in Finland and the Finnish Grid and Cloud Infrastructure (persistent identifier urn:nbn:fi:research-infras-2016072533).

Notes and references

‡ Related intramolecular cyclisation is used in organic syntheses, e.g. for the preparation of aromatic compounds with a 1,4-phenoxazine structure.[7,51–55]

1 R. V. Slone, D. I. Yoon, R. M. Calhoun and J. T. Hupp, *J. Am. Chem. Soc.*, 1995, **117**, 11813–11814.
2 O. Kahn, J. Kröber and C. Jay, *Adv. Mater.*, 1992, **4**, 718–728.
3 A. L. Zelikoff, J. Kopilov, I. Goldberg, G. W. Coates and M. Kol, *Chem. Commun.*, 2009, 6804–6806.
4 K. J. Blackmore, N. Lal, J. W. Ziller and A. F. Heyduk, *J. Am. Chem. Soc.*, 2008, **130**, 2728–2729.
5 K. J. Blackmore, N. Lal, J. W. Ziller and A. F. Heyduk, *Eur. J. Inorg. Chem.*, 2009, 735–743.
6 M. M. Hänninen, P. Paturi, H. M. Tuononen, R. Sillanpää and A. Lehtonen, *Inorg. Chem.*, 2013, **52**, 5714–5721.
7 F. D. Lesh, R. L. Lord, M. J. Heeg, H. B. Schlegel and C. N. Verani, *Eur. J. Inorg. Chem.*, 2012, 463–466.
8 P. Chaudhuri, M. Hess, J. Müller, K. Hildenbrand, E. Bill, T. Weyhermüller and K. Wieghardt, *J. Am. Chem. Soc.*, 1999, **121**, 9599–9610.
9 W. Kaim and B. Schwederski, *Coord. Chem. Rev.*, 2010, **254**, 1580–1588.
10 W. Kaim, *Inorg. Chem.*, 2011, **50**, 9752–9765.
11 Y. Wang, J. Li, L. Zhang, C. Chen, R. Feng, Y. Zhao, Y. Q. Zhang, G. Tan, Y. Song and X. Wang, *Dalt. Trans.*, 2018, **47**, 17211–17215.

12 E. Evangelio and D. Ruiz-Molina, *Eur. J. Inorg. Chem.*, 2005, 2957–2971.

13 W. Nicolazzi and A. Bousseksou, *Comptes Rendus Chim.*, 2018, **21**, 1060–1074.

14 O. Cador, F. Chabre, A. Dei, C. Sangregorio, J. Van Slageren and M. G. F. Vaz, *Inorg. Chem.*, 2003, **42**, 6432–6440.

15 A. Caneschi, A. Cornia and A. Dei, *Inorg. Chem.*, 1998, **37**, 3419–3421.

16 D. Ruiz-Molina, K. Wurst, D. N. Hendrickson, C. Rovira and J. Veciana, *Adv. Funct. Mater.*, 2002, **12**, 347–351.

17 D. Ruiz-Molina, J. Veciana, K. Wurst, D. N. Hendrickson and C. Rovira, *Inorg. Chem.*, 2000, **39**, 617–619.

18 A. Rajput, A. K. Sharma, S. K. Barman, D. Koley, M. Steinert and R. Mukherjee, *Inorg. Chem.*, 2014, **53**, 36–48.

19 H. Hagiwara, T. Masuda, T. Ohno, M. Suzuki, T. Udagawa and K.-I. Murai, , DOI:10.1021/acs.cgd.7b01141.

20 A. Lennartson, A. D. Bond, S. Piligkos and C. J. McKenzie, *Angew. Chemie - Int. Ed.*, 2012, **51**, 11049–11052.

21 K. Senthil Kumar, Y. Bayeh, T. Gebretsadik, F. Elemo, M. Gebrezgiabher, M. Thomas and M. Ruben, *Dalt. Trans.*, 2019, **48**, 15321–15337.

22 K. Dankhoff, C. Lochenie and B. Weber, *Molecules*, 2020, **25**, 581.

23 S. Schönfeld, C. Lochenie, P. Thoma and B. Weber, *CrystEngComm*, 2015, **17**, 5389–5395.

24

25 G. M. Sheldrick, *Acta Crystallogr. Sect. A Found. Crystallogr.*, 2007, **64**, 112–122.

26 G. M. Sheldrick, *Acta Crystallogr. Sect. C Struct. Chem.*, 2015, **71**, 3–8.

27 O. V. Dolomanov, L. J. Bourhis, R. J. Gildea, J. A. K. Howard and H. Puschmann, *J. Appl. Crystallogr.*, 2009, **42**, 339–341.

28 F. Neese, *Wiley Interdiscip. Rev. Comput. Mol. Sci.*, 2018, **8**, 4–9.

29 F. Neese, F. Wennmohs, U. Becker and C. Riplinger, *J. Chem. Phys.*, 2020, **152**, 224108.

30 J. P. Perdew, K. Burke and M. Ernzerhof, *Phys. Rev. Lett.*, 1996, **78**, 1396.

31 J. P. Perdew, K. Burke and M. Ernzerhof, *Phys. Rev. Lett.*, 1996, **77**, 3865–3868.

32 T. Yanai, D. P. Tew and N. C. Handy, *Chem. Phys. Lett.*, 2004, **393**, 51–57.

33 A. Becke, *Phys. Rev. A*, 1988, **38**, 3098–3100.

34 C. Lee, W. Yang and R. G. Parr, *Phys. Rev. B*, 1988, **37**, 785–789.

35 M. Douglas and N. M. Kroll, *Ann. Phys. (N. Y).*, 1974, **82**, 89–155.

36 B. A. Hess, *Phys. Rev. A*, 1986, **33**, 3742–3748.

37 D. A. Pantazis, X.-Y. Chen, C. R. Landis and F. Neese, *J. Chem. Theory Comput.*, 2008, **4**, 908–919.

38 F. Weigend and R. Ahlrichs, *Phys. Chem. Chem. Phys.*, 2005, **7**, 3297–3305.

39 R. Mukherjee, *Inorg. Chem.*, 2020, **59**, 12961–12977.

40 S. N. Brown, *Inorg. Chem.*, 2012, **51**, 1251–1260.

41 M. K. Hossain, M. Haukka, M. M. Hänninen, G. C. Lisensky, P. Paturi, E. Nordlander and A. Lehtonen, *Inorg. Chem. Commun.*, 2018, **93**, 149–152.

42 E. Salojärvi, A. Peuronen, M. Lahtinen, H. Huhtinen, L. S. Vlasenko, M. Lastusaari and A. Lehtonen, *Molecules*, 2020, **25**, 1–17.

43 F. D. Lesh, R. L. Lord, M. J. Heeg, H. B. Schlegel and C. N. Verani, *Eur. J. Inorg. Chem.*, 2012, 463–466.

44 W. Phonsri, D. S. Macedo, K. R. Vignesh, G. Rajaraman, C. G. Davies, G. N. L. Jameson, B. Moubaraki, J. S. Ward, P. E. Kruger, G. Chastanet and K. S. Murray, *Chem. - A Eur. J.*, 2017, **23**, 7052–7065.

45 A. Abragam and B. Bleaney, *Electron Paramagnetic Resonance of Transition Ions; Dover Publications*, Dover Publications, New York, 1986.

46 A. Ozarowski, S. A. Zvyagin, W. M. Reiff, J. Telser, L. C. Brunel and J. Krzystek, *J. Am. Chem. Soc.*, 2004, **126**, 6574–6575.

47 M. P. Hendrich and P. G. Debrunner, *Biophys. J.*, 1989, **56**, 489–506.

48 S. Tewary, I. A. Gass, K. S. Murray and G. Rajaraman, , DOI:10.1002/ejic.201201077.

49 L. Salmon, A. Bousseksou, B. Donnadieu and J.-P. Tuchagues, , DOI:10.1021/ic048387k.

50 I. S. ˇ Alitroš, R. Boča,] L'ubor Dlháň, M. Gembický, J. Kožíšek, J. Linares, J. Moncol', I. Nemec, L. Perašínová, F. Renz, I. Svoboda and H. Fuess, , DOI:10.1002/ejic.200900169.

51 S. S. Bag, S. Ghorai, S. Jana and C. Mukherjee, *RSC Adv.*, 2013, **3**, 5374–5377.

52 L. A. Farmer, E. A. Haidasz, M. Griesser and D. A. Pratt, *J. Org. Chem.*, 2017, **82**, 10523–10536.

53 L. G. Ranis, K. Werellapatha, N. J. Pietrini, B. A. Bunker and S. N. Brown, *Inorg. Chem.*, 2014, **53**, 10203–10216.

54 A. I. Poddel'Sky, V. K. Cherkasov, M. P. Bubnov, L. G. Abakumova and G. A. Abakumov, *J. Organomet. Chem.*, 2005, **690**, 145–150.

55 E. P. Ivakhnenko, P. A. Knyazev, K. A. Lyssenko, A. G. Starikov and V. I. Minkin, *Inorganica Chim. Acta*, 2019, **484**, 430–436.